Discover Oncology

Analysis

Methuosis key gene ARF6 as a diagnostic, prognostic and immunotherapeutic marker for prostate cancer: based on a comprehensive pan-cancer multi-omics analysis

Yongjin Yang[1,2] · Liangliang Qing[3] · Chengyu You[1,2] · Qingchao Li[1,2] · Wenbo Xu[1,2] · Zhilong Dong[1,2]

Received: 14 February 2025 / Accepted: 1 April 2025
Published online: 23 May 2025
© The Author(s) 2025 OPEN

Abstract

Background Prostate cancer (PCa) is a leading cause of cancer-related mortality among men worldwide. Despite progress in the understanding of tumor biology, the prognosis for advanced prostate cancer remains poor, necessitating the identification of novel diagnostic, prognostic, and therapeutic biomarkers. Methuosis, a recently identified form of programmed cell death (PCD), is characterized by cytoplasmic vacuole accumulation and subsequent cell rupture, distinct from classical apoptosis and necrosis. The key regulatory gene in Methuosis, ARF6 (ADP-ribosylation factor 6), has emerged as a potential marker for cancer diagnosis and treatment. However, its role in prostate cancer and other malignancies remains insufficiently understood.

Methods In this study, we performed a comprehensive pan-cancer multi-omics analysis to investigate the role of ARF6 in Methuosis across multiple cancer types, with a specific focus on PCa as the primary context. Using data from public databases, including RNA sequencing, gene expression profiling, and clinical outcomes, we assessed the association between ARF6 expression and patient prognosis in PCa within this broader pan-cancer framework. Additionally, we employed functional enrichment analyses and survival analysis to explore the potential of ARF6 as a diagnostic and prognostic marker for prostate cancer. Immunotherapy-related gene expression signatures were also evaluated to determine the therapeutic relevance of ARF6.

Results ARF6 was significantly overexpressed in PCa tissues compared to normal tissues and was associated with poor prognosis ($p < 0.05$), particularly in advanced and metastatic stages. Receiver operating characteristic (ROC) analysis revealed a diagnostic AUC of 0.792 for ARF6. Functional analyses indicated that ARF6 regulates pathways critical to cell migration, invasion, and drug resistance. Moreover, ARF6 expression showed a strong negative correlation with immune checkpoint markers, such as PD-L1 ($r = -0.74$), suggesting its potential as an immunotherapy target. These findings underscore ARF6's pivotal role in Methuosis and its promise as a biomarker in PCa.

Conclusion ARF6 is a key regulator of Methuosis in prostate cancer, contributing to tumor progression, metastasis, and resistance to treatment. Our findings support the potential of ARF6 as a diagnostic, prognostic, and immunotherapeutic target in prostate cancer. Further experimental validation is needed to confirm these observations and to explore the therapeutic implications of targeting ARF6 in cancer treatment.

Keywords Prostate cancer · Methuosis · ARF6 · Programmed cell death · Biomarkers · Immunotherapy · Multi-omics · Pan-cancer analysis · Drug resistance · Prognosis

✉ Zhilong Dong, dzl19780829@163.com | [1]Department of Urology, the Second Hospital & Clinical Medical School, Lanzhou University, Lanzhou 730000, Gansu, China. [2]Gansu Province Clinical Research Center for Urinary System Disease, Lanzhou 730000, Gansu, China. [3]Department of Urology, Zigong Fourth People's Hospital, No.19 Tanmulin Street, Ziliujing District, Zigong 643000, China.

1 Introduction

Prostate cancer (PCa) is one of the most common malignancies affecting men globally, representing a significant burden on public health [1, 2]. Despite advances in early detection and therapeutic strategies, the prognosis for patients with advanced or metastatic prostate cancer remains poor, underscoring the need for innovative biomarkers and therapeutic approaches [3–5]. Recent studies have brought attention to the complex biological mechanisms underlying cancer progression, among which programmed cell death (PCD) plays a pivotal role in regulating tumor initiation, growth, and metastasis [6–8]. Conventional PCD mechanisms, including apoptosis, autophagy, and necrosis, have been extensively studied [9–12]. However, emerging evidence suggests that novel forms of PCD, such as Methuosis, are equally crucial in shaping cancer biology, yet remain underexplored [13–15].

Methuosis is a newly identified form of programmed cell death, distinct from traditional apoptotic and necrotic pathways. Characterized by the accumulation of vacuoles in the cytoplasm and subsequent cellular rupture, Methuosis has been implicated in various cancer types [16, 17]. Unlike apoptosis, which typically involves caspase activation and controlled cell death, Methuosis relies on excessive cytoplasmic vacuole accumulation derived from macropinosomes, leading to catastrophic membrane rupture and cell death [18, 19]. In contrast to necrosis, which is typically an uncontrolled inflammatory process, Methuosis operates as a regulated pathway, often triggered by disruptions in endosomal trafficking. This form of cell death is particularly relevant to tumors that exhibit resistance to traditional therapeutic modalities [20]. Given its unique characteristics, Methuosis presents a potential therapeutic target for cancer treatment, as well as a novel biomarker for diagnosis and prognosis.

Among the key regulatory players in Methuosis, ARF6 (ADP-ribosylation factor 6) has recently emerged as a central gene influencing this form of cell death [21]. ARF6, a small GTPase involved in cellular trafficking, membrane dynamics, and vesicle formation, has been implicated in several cellular processes critical to tumor progression, including invasion, migration, and drug resistance [22, 23]. Recent studies have highlighted ARF6's role in the initiation and regulation of Methuosis, positioning it as a potential diagnostic, prognostic, and therapeutic marker in cancer [24, 25]. However, the mechanistic understanding of ARF6 in the context of Methuosis and its association with prostate cancer is still in its nascent stages.

In this study, we aim to conduct a comprehensive pan-cancer multi-omics analysis to elucidate the role of ARF6 in Methuosis across different cancer types, with a particular focus on prostate cancer. Using data from The Cancer Genome Atlas (TCGA), Genotype-Tissue Expression (GTEx), and other publicly available databases, we systematically analyzed ARF6 expression patterns, mutational landscape, and chromatin accessibility across various cancer types. We further explored its correlation with immune cell infiltration, chemotherapy sensitivity, and key signaling pathways, with a particular focus on prostate cancer. Our findings reveal that ARF6 is not only a potential diagnostic and prognostic marker but also a promising target for immunotherapy in prostate cancer. Through this analysis, we hope to contribute to the growing body of evidence surrounding Methuosis and ARF6, paving the way for new therapeutic strategies in prostate cancer and other malignancies.

2 Methods

2.1 Comprehensive data collection and processing across cancers

We collected pan-cancer data on ARF6 expression and related clinical features from The Cancer Genome Atlas (TCGA, http://cancergenome.nih.gov/) and Genotype-Tissue Expression (GTEx, https://gtexportal.org/home/) databases through the UCSC Xena platform. Additionally, we analyzed the correlation between ARF6 expression and the tumor immune microenvironment using various immune infiltration algorithms from the TIMER2.0 database (http://timer.cistrome.org). We also integrated multiple single-cell datasets from the TISCH database (http://tisch.comp-genomics.org/home).

2.2 ARF6 expression localization and subcellular distribution in pan-cancer

This study utilized transcriptome data from the Human Protein Atlas (HPA) v23.0 (http://www.proteinatlas.org) and Genotype-Tissue Expression (GTEx) v8 (dbGaP Accession: phs000424.v8.p2) databases. Gene ID matching and annotation

standardization were performed using Ensembl release 109. A gene expression profile was constructed for 50 anatomical tissue types. The normalization of expression data was based on the maximum nTPM (Normalized Transcripts Per Million) value for each gene in both HPA and GTEx datasets. For complex organs with multiple sub-tissues (such as brain regions, lymphoid tissues, and the intestine), the maximum nTPM value from all sub-tissues was used to represent the overall expression feature. The data normalization process followed the official HPA procedure, where RSEM was used to quantify gene expression, followed by TPM normalization and log2(TPM + 1) transformation. The results were visualized using a lollipop plot, with the X-axis representing tissue types categorized by anatomical systems, and the Y-axis showing log2(nTPM + 1) values. The size and color gradient of the points represent the original nTPM range (0–100). A threshold of nTPM ≥ 1.0 was used to define significant tissue-specific expression. To increase the sample size of normal tissues, we paired normal samples from GTEx with tumor samples from TCGA and transformed the data into unit-free Z-scores using $(x-\mu)/\sigma$ for comparison. Organ maps were created using the gganatogram package to display median Z-scores of different tissues and tumors compared to normal groups.

2.3 ARF6 expression and survival analysis

Survival data were obtained from the TCGA database, and the relationship between ARF6 expression and prognostic indicators (including progression-free interval (PFI) and disease-free interval (DFI)) was analyzed using the"survival"and"surv"R packages. Univariate Cox proportional hazards regression analysis was performed using the"coxph"function to evaluate the association between ARF6 expression (as a continuous variable) and survival outcomes, with HR and 95% CI calculated to assess risk. To account for potential confounders, multivariate Cox regression was also conducted, adjusting for clinical variables such as age, tumor stage, and Gleason score, sourced from TCGA metadata. Cox regression analysis was performed, and the results were visualized using the"forest plot"package in R (version 2.0.1), with statistical significance denoted by $p < 0.05$. Tumor samples were classified into high and low expression groups based on median values of ARF6 mRNA expression (log2-transformed TPM), and the proportions of each subtype were calculated. The significance of these differences was assessed using Chi-square tests, implemented via the"chisq.test"function in R, to compare subtype distributions across survival groups.

2.4 Single-cell tumor immune microenvironment across cancers

For each designated tumor type, Pearson correlation analysis between immune genes and ARF6 expression was conducted using the cor.test function, and heatmaps were generated using the ComplexHeatmap package. Single-cell transcriptome data across cancer types from the TISCH database were integrated to create cross-cancer single-cell expression heatmaps using the pheatmap tool. Data preprocessing involved Z-score normalization, followed by calculation of sample similarity using the Euclidean distance matrix, and optimization of row and column topological structures using the Ward hierarchical clustering algorithm. This multi-dimensional visualization strategy effectively revealed the specific expression patterns of cell subpopulations in the tumor microenvironment. Additionally, we performed Spearman correlation analysis to explore the relationship between ARF6 expression and immune-related expression features. The cor.test function in R was used for correlation calculations with datasets from 68 immune-related features, and results were visualized using the hplot1 function from the fromto package.

2.5 Pan-cancer pathway enrichment analysis

We utilized the CancerSEA database, which organizes 14 functional states of tumor cells. Using the GSVA package with the zscore parameter, we calculated the z-scores for these functional state gene sets and obtained combined z-scores. The scale function was used to further standardize the scores, and Pearson correlation analysis was performed between the gene expression and the scores of each gene set.

2.6 Pan-cancer mutation analysis

The correlation between ARF6 gene expression and scores for Aneuploidy, Homologous Recombination Defects, and other features was calculated using the cor.test function, and the results were visualized using a radar chart generated by the fmsb package. To calculate mutation frequency, SNV data from 33 cancer types (n = 8663) were collected from the TCGA database. The SNV data included multiple mutation types such as Missense Mutation, Silent, 5'flap, 3'UTR, RNA, In_Frame_Del, Nonsense Mutation, Splice Site, Intron, 5'UTR, In_Frame_Ins, Frame Shift Del, Nonstop Mutation, 3'flap, Frame Shift Ins, and Translation Start Site. Oncoplot diagrams were generated using the maftools package.

2.7 Pan-cancer drug sensitivity and immunotherapy analysis

Chemotherapy data were obtained from the GDSC database (https://www.cancerrxgene.org/) and the CTRP database (http://portals.broadinstitute.org/ctrp/), and the interaction between ARF6 expression and drug sensitivity was analyzed. Spearman correlation analysis was performed using the cor.test function to calculate the relationship between ARF6 and different chemotherapy drugs. Additionally, based on the PRAD dataset, the Kruskal–Wallis rank sum test was used to compare the statistical differences in ARF6 expression between different treatment response groups.

2.8 ARF6 expression and immune function in prostate cancer

To assess MeTIL characteristics, we performed principal component analysis (PCA) to convert the single methylation values of MeTIL markers into MeTIL scores and transformed the data into Z-scores using $(x-\mu)/\sigma$. Based on the median value of ARF6, samples were divided into high and low expression groups, and the statistical differences in MeTIL scores between the two groups were analyzed using the Wilcoxon rank sum test. Furthermore, the TIP (Tracking Tumor Immunophenotype) server was used to integrate the"ssGSEA"and"CIBERSORT"methods to analyze and visualize anti-cancer immune states and tumor-infiltrating immune cells across the seven-step cancer immune cycle. The TIP database quantifies immune response scores for each step based on gene expression data, and Spearman correlation analysis was performed to assess the relationship between gene expression and immune response scores, with visualization using the linkET package. Immune cell content differences between high and low expression groups were compared using the Wilcoxon rank sum test, and changes in immune cells were displayed using heatmaps.

2.9 ATAC-seq analysis

To study the chromatin accessibility patterns associated with ARF6, ATAC-seq data were analyzed. Raw reads were aligned to the hg19 genome using Bowtie2, and duplicates were removed using Picard Tools. Peaks were called using MACS2 ($q < 0.05$), and genomic features such as promoters, exons, and introns were annotated using the ChIPseeker package in R. Promoter regions were defined as ± 1 kb and 1–2 kb from transcription start sites (TSS). Chromosomal distribution and peak size distribution were visualized using GenomicRanges and ggplot2, and the enrichment of accessible regions in specific genomic contexts was plotted based on the percentage of peaks in each feature category.

2.10 Validation of ARF6 expression by RT-qPCR

To validate the bioinformatics findings, ARF6 mRNA expression levels were assessed in prostate cancer cell lines (LNCaP and PC- 3) and a normal prostate epithelial cell line (RWPE- 1). Cells were cultured in RPMI- 1640 medium (Gibco) supplemented with 10% fetal bovine serum (FBS) and 1% penicillin–streptomycin at 37 °C with 5% CO_2. Total RNA was extracted using TRIzol reagent (Invitrogen) according to the manufacturer's instructions. RNA integrity was confirmed by agarose gel electrophoresis, and 1 μg of RNA was reverse-transcribed into cDNA using the PrimeScript RT Reagent Kit (Takara). Quantitative real-time PCR (RT-qPCR) was performed on a Bio-Rad CFX96 system using SYBR Green Master Mix (Applied Biosystems) with the following primers: ARF6 forward, 5'-CCATCCCTGAAGGAGAGA- 3'; ARF6 reverse, 5'-TCCCGC CAAACTGTAGAAC- 3'; GAPDH forward, 5'-AGAGGCCTCCACACTCTTTC- 3'; GAPDH reverse, 5'-AGGCGCCATCCACAGTCT TC- 3' (used as an internal control). The reaction conditions included an initial denaturation at 95 °C for 10 min, followed

by 40 cycles of 95 °C for 15 s and 58 °C for 1 min. Relative ARF6 expression levels were calculated using the 2^-ΔΔCt method, normalized to GAPDH, with RWPE- 1 as the reference sample. Experiments were performed in triplicate, and statistical significance was determined using a two-tailed Student's t-test ($p < 0.05$).

2.11 Statistical analysis

All data were processed using R software (V.4.3.0). Pearson correlation analysis was applied to normally distributed data, and Spearman correlation analysis was used for non-normally distributed data. Kruskal–Wallis rank sum tests, Wilcoxon rank sum tests, and sign rank tests were used to identify differences between variables. The"survival"R package was used for Cox regression and Kaplan–Meier survival analysis, with log-rank tests assessing statistical significance. The"survminer"R package was used to visualize Kaplan–Meier analysis results, and the relative hazard ratios (HR) and 95% confidence intervals (CI) were reported. ROC analysis was performed using the"pROC"R package to evaluate the predictive power of the models. All statistical tests were two-tailed, and a p-value < 0.05 was considered statistically significant. A p-value < 0.0001 was considered highly significant (*p < 0.05, **p < 0.01, ***p < 0.001, ****p < 0.0001).

3 Result

3.1 Expression landscape of ARF6 across tissues, cell types, and cancer contexts

The expression landscape of ARF6 was systematically analyzed using transcriptomic data from the Human Protein Atlas (HPA), Genotype-Tissue Expression (GTEx), and The Cancer Genome Atlas (TCGA). In cancer cell lines, ARF6 exhibited variable expression levels across different tumor types, with certain cancers showing notably higher or lower expression, suggesting potential tumor-specific roles of ARF6 in cancer biology (Fig. 1A). In immune cells, ARF6 expression was heterogeneous, with distinct expression patterns observed in various immune cell populations, such as higher expression in monocytes and lower expression in T cells, indicating its potential involvement in immune cell function and regulation (Fig. 1B). Across normal tissues, ARF6 displayed tissue-specific expression profiles, with higher expression observed in tissues such as the brain and liver, while lower expression was noted in others like the heart and skeletal muscle, reflecting its potential functional diversity in different tissue contexts (Fig. 1C). At the single-cell level, ARF6 expression further demonstrated cell-type-specific patterns, with significant expression in epithelial cells and fibroblasts, but lower levels in endothelial cells, highlighting its potential roles in diverse cellular processes (Fig. 1D). Furthermore, analysis of ARF6 expression in tumors from the TCGA database, normalized using Z-scores and filtered for outliers (Z-scores < – 3 or > 3), revealed significant differential expression between tumor and normal tissues across multiple cancer types. Wilcoxon Rank Sum Tests were used to assess the statistical significance of these differences, and the results indicated that ARF6 was frequently dysregulated in tumors, with both upregulation and downregulation observed depending on the cancer type, suggesting its potential involvement in tumorigenesis (Fig. 1E). Together, these findings provide a comprehensive overview of ARF6 expression across various biological contexts, underscoring its potential roles in normal tissue function, immune regulation, and cancer development.

3.2 ARF6 diagnostic and prognostic significance in cancer

The diagnostic performance of ARF6 in distinguishing tumor tissues from normal tissues was assessed using Receiver Operating Characteristic (ROC) curve analysis, which demonstrated that ARF6 has a strong diagnostic capability, particularly in PRAD (prostate adenocarcinoma), where the AUC value was notably high, indicating excellent diagnostic performance (Fig. 2A). To expand the normal sample size, ARF6 expression data from GTEx normal tissues were paired with TCGA tumor data, and Z-scores were calculated to standardize expression values using the formula $(x-\mu)/\sigma$, where x is the expression value, μ is the mean, and σ is the standard deviation. Visualization of median Z-scores across organs revealed distinct expression patterns between tumor and normal tissues, with significant differences observed in organs such as the liver and prostate (Fig. 2B).Logistic regression analysis, performed using a binomial model, identified significant associations between ARF6 expression and tumor status. Notably, ARF6 expression showed a strong positive association with PRAD (OR = 3.090[95%CI: 2.174–4.392], p = 3.157980e- 10), highlighting its potential role in the development and progression of this cancer type. Additionally, ARF6 exhibited a significant negative association with READ (OR = 0.181[95%CI: 0.068–0.486], p = 6.770936e- 04),

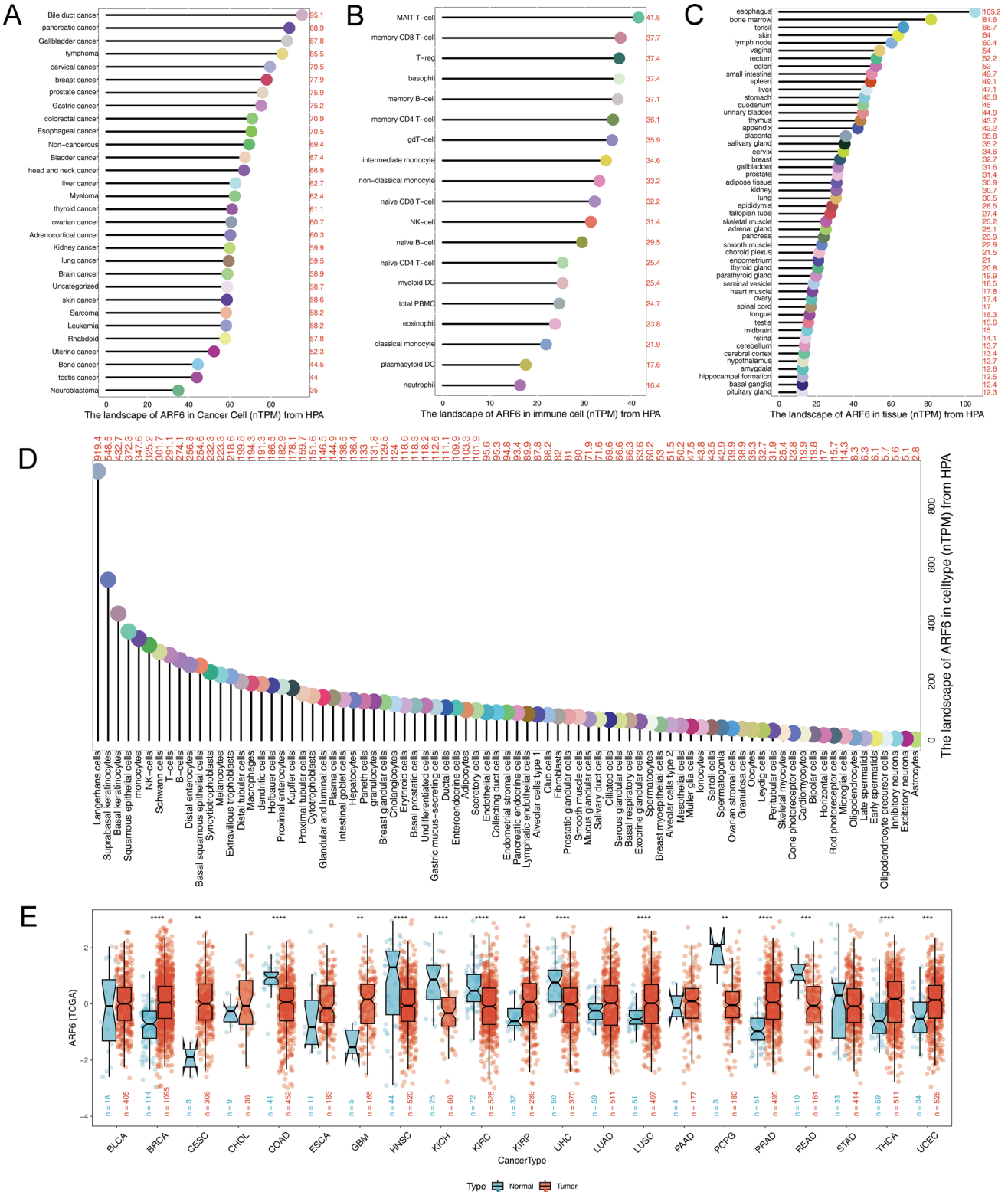

Fig. 1 Expression profiles of ARF6 in various contexts. **A** ARF6 expression in cancer cell lines (HPA data). **B** ARF6 expression in immune cell populations (HPA data). **C** ARF6 expression across normal tissues (HPA and GTEx data). **D** ARF6 expression at the single-cell level (HPA data). **E** Differential ARF6 expression between tumor and normal tissues (TCGA data), analyzed using Z-scores and Wilcoxon Rank Sum Tests. Outliers (Z-scores < − 3 or > 3) were removed. to assess statistical significance (* indicates $p < 0.05$; ** indicates $p < 0.01$; *** indicates $p < 0.005$; **** indicates $p < 0.001$). Expression differences are shown as boxplots, with each dot representing a sample

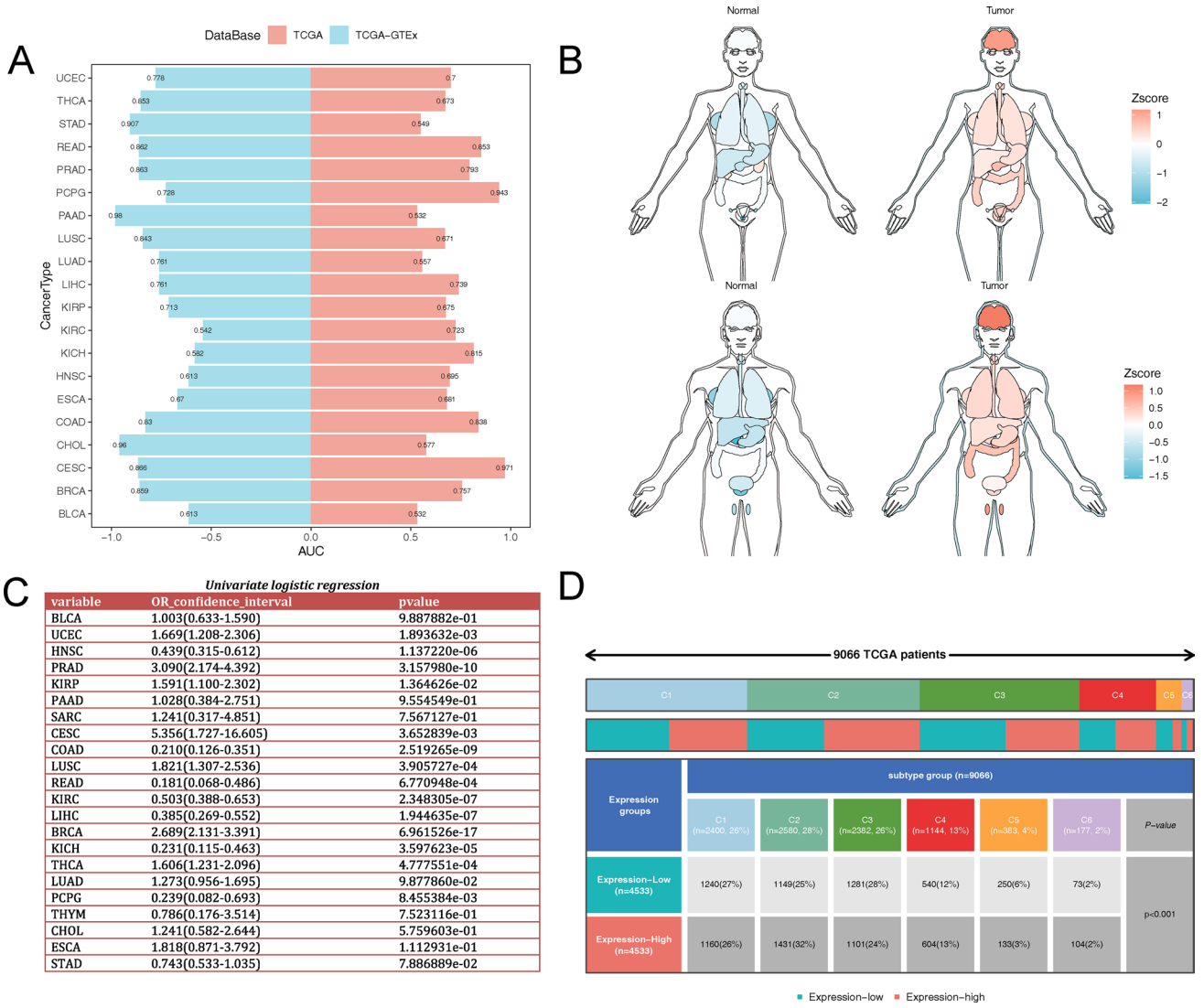

variable	OR_confidence_interval	pvalue
BLCA	1.003(0.633-1.590)	9.887882e-01
UCEC	1.669(1.208-2.306)	1.893632e-03
HNSC	0.439(0.315-0.612)	1.137220e-06
PRAD	3.090(2.174-4.392)	3.157980e-10
KIRP	1.591(1.100-2.302)	1.364626e-02
PAAD	1.028(0.384-2.751)	9.554549e-01
SARC	1.241(0.317-4.851)	7.567127e-01
CESC	5.356(1.727-16.605)	3.652839e-03
COAD	0.210(0.126-0.351)	2.519265e-09
LUSC	1.821(1.307-2.536)	3.905727e-04
READ	0.181(0.068-0.486)	6.770948e-04
KIRC	0.503(0.388-0.653)	2.348305e-07
LIHC	0.385(0.269-0.552)	1.944635e-07
BRCA	2.689(2.131-3.391)	6.961526e-17
KICH	0.231(0.115-0.463)	3.597623e-05
THCA	1.606(1.231-2.096)	4.777551e-04
LUAD	1.273(0.956-1.695)	9.877860e-02
PCPG	0.239(0.082-0.693)	8.455384e-03
THYM	0.786(0.176-3.514)	7.523116e-01
CHOL	1.241(0.582-2.644)	5.759603e-01
ESCA	1.818(0.871-3.792)	1.112931e-01
STAD	0.743(0.533-1.035)	7.886889e-02

Fig. 2 ARF6 Diagnostic and Prognostic Significance in Cancer. **A** ROC curve analysis showing the diagnostic performance of ARF6 in distinguishing tumor from normal tissues, with a focus on PRAD. **B** Median Z-scores of ARF6 expression in tumor and normal tissues across various organs, visualized using organ-specific plots. **C** Logistic regression analysis of ARF6 expression in tumor versus normal tissues, highlighting significant associations, particularly in PRAD. **D** Distribution of tumor subtypes in high and low ARF6 expression groups, assessed using Chi-square tests

suggesting its potential as a protective factor or differential expression pattern in this cancer type. Positive associations were also observed in UCEC (OR = 1.669[95%CI: 1.208–2.306], p = 1.893522e- 03) and BRCA (OR = 2.689[95%CI: 2.131–3.391], p = 6.961526e- 17), while negative associations were noted in COAD (OR = 0.210[95%CI: 0.126–0.351], p = 2.519265e- 09) and LIHC (OR = 0.385[95%CI: 0.269–0.552], p = 1.944635e- 07) (Fig. 2C). Furthermore, stratification of tumor samples into high and low ARF6 expression groups based on median expression values revealed significant differences in the distribution of tumor subtypes, as assessed by Chi-square tests ($p < 0.001$). For example, in the high ARF6 expression group, a higher proportion of PRAD and BRCA tumors was observed, while the low ARF6 expression group showed a higher proportion of COAD and READ tumors, suggesting that ARF6 expression levels may influence tumor subtype composition (Fig. 2D). These findings underscore the potential of ARF6 as a diagnostic marker and its significant role in tumor biology across various cancer types, with particularly strong diagnostic performance in PRAD and a notable association with PRAD.

Discover Oncology (2025) 16:882 | https://doi.org/10.1007/s12672-025-02275-y

Fig. 3 Single-Cell and Spatial Transcriptomic Analysis of Tumor Microenvironment across Cancer Types. **A** Cross-cancer single-cell expression heatmap constructed using TISCH database data. Z-score normalization and hierarchical clustering revealed significant heterogeneity in ARF6 expression. **B** Spatial transcriptomic analysis of tumor tissue slices from the Sparkle database

3.3 Single-cell and spatial transcriptomic analysis of tumor microenvironment across cancer types

This study integrated cross-cancer single-cell transcriptomic data from the TISCH database to construct a cross-cancer single-cell expression heatmap using the pheatmap tool (Fig. 3A). The data was preprocessed using Z-score normalization, and Euclidean distance matrices were calculated to assess sample similarity. The Ward hierarchical clustering algorithm was applied to optimize the row and column topological structure of the heatmap. This multi-dimensional visualization strategy effectively revealed the cell-type-specific expression patterns across various cancer types and their tumor microenvironments (TME). Quantitative analysis showed that ARF6 gene expression exhibited significant tissue and cell-type heterogeneity. In prostate cancer (PRAD), the ARF6 expression was notably elevated, particularly in tumor cell subpopulations, which may be closely associated with tumor cell migration and immune evasion mechanisms in PRAD. Furthermore, the differential expression of ARF6 in immune cell subpopulations, such as T cells and dendritic cells, emphasized its potential functional role in the TME of various cancers, particularly in PRAD.

To further explore the spatial transcriptomic features of tumor tissues, we employed the Sparkle database to conduct spatial transcriptomic analysis on multiple tumor tissue slices (Fig. 3B). The Sparkle database integrates 10 ×Visium sequencing data to construct a pan-cancer spatial transcriptome atlas. In this analysis, cell types within each micro-region were characterized, and micro-regions were named based on the proportion of cell types present. For instance, micro-regions dominated by malignant cells were termed "malignant cell micro-regions," while those with a high proportion of endothelial cells were named "endothelial cell micro-regions." We then examined the average gene expression levels in each micro-region and applied Z-score normalization using the scale function in R to enhance the comparability of data across different tissue slices. The normalized data was visualized using the pheatmap package, clearly presenting the gene expression patterns within different micro-regions. In PRAD tissues, the malignant cell micro-regions exhibited significantly higher gene expression compared to normal tissue regions, especially for genes involved in cell proliferation, immune evasion, and tumor metabolism. This analysis revealed the spatial distribution and complex gene expression patterns within the TME of prostate cancer.

3.4 Correlation of ARF6 expression with immune-related genes and immune cell infiltration across tumors

In this section, all reported correlation coefficients are derived from statistical tests with a significance threshold of $p < 0.05$, ensuring robust and reliable associations between ARF6 expression and immune-related features across cancer types. The correlation between ARF6 expression and immune-related genes was analyzed across various cancer types using Pearson's correlation method. The heatmap generated (Fig. 4A) illustrates the relationships, with red indicating positive correlations and blue indicating negative correlations. The depth of the color corresponds to the absolute value of the correlation coefficient, with darker colors reflecting stronger correlations. In prostate cancer (PRAD), ARF6 exhibited a strong positive correlation with immune-related genes such as CD8 A ($r = 0.78$) and PDCD1 ($r = 0.65$), suggesting that ARF6 may influence immune cell infiltration and checkpoint activity in the TME. On the other hand, a notable negative correlation was observed between ARF6 and the immunosuppressive gene TGFB1 ($r = -0.72$), particularly in cancers like colon adenocarcinoma (COAD), highlighting the potential differential regulatory effects of ARF6 in various tumor environments.

In the second analysis, Spearman's correlation was applied to explore the relationship between ARF6 expression and immune cell infiltration levels across different cancers (Fig. 4B). The heatmap shows the Spearman correlation between ARF6 and immune cell types, where red represents positive correlations and blue represents negative correlations, with the intensity of the color indicating the strength of the correlation. In PRAD, a strong positive correlation was found between ARF6 expression and CD8 +T cells ($r = 0.84$), macrophages ($r = 0.79$), and dendritic cells ($r = 0.72$), indicating that ARF6 may facilitate the infiltration of these immune cells, which are critical for anti-tumor immunity. Conversely, in tumors such as lung adenocarcinoma (LUAD), ARF6 showed a weaker negative correlation with regulatory T cells ($r = -0.60$), suggesting that ARF6 might have an immune-modulatory role specific to each cancer type.

Finally, to explore the relationship between ARF6 and a broader set of immune-related features, we used data from 68 immune-related expression traits retrieved from the UCSC Xena database (Fig. 4C). Spearman's correlation analysis revealed strong negative correlations between ARF6 expression and various immune-related markers in PRAD, including markers of immune evasion such as PD-L1 ($r = -0.74$) and immunosuppressive cytokines like IL10 (r

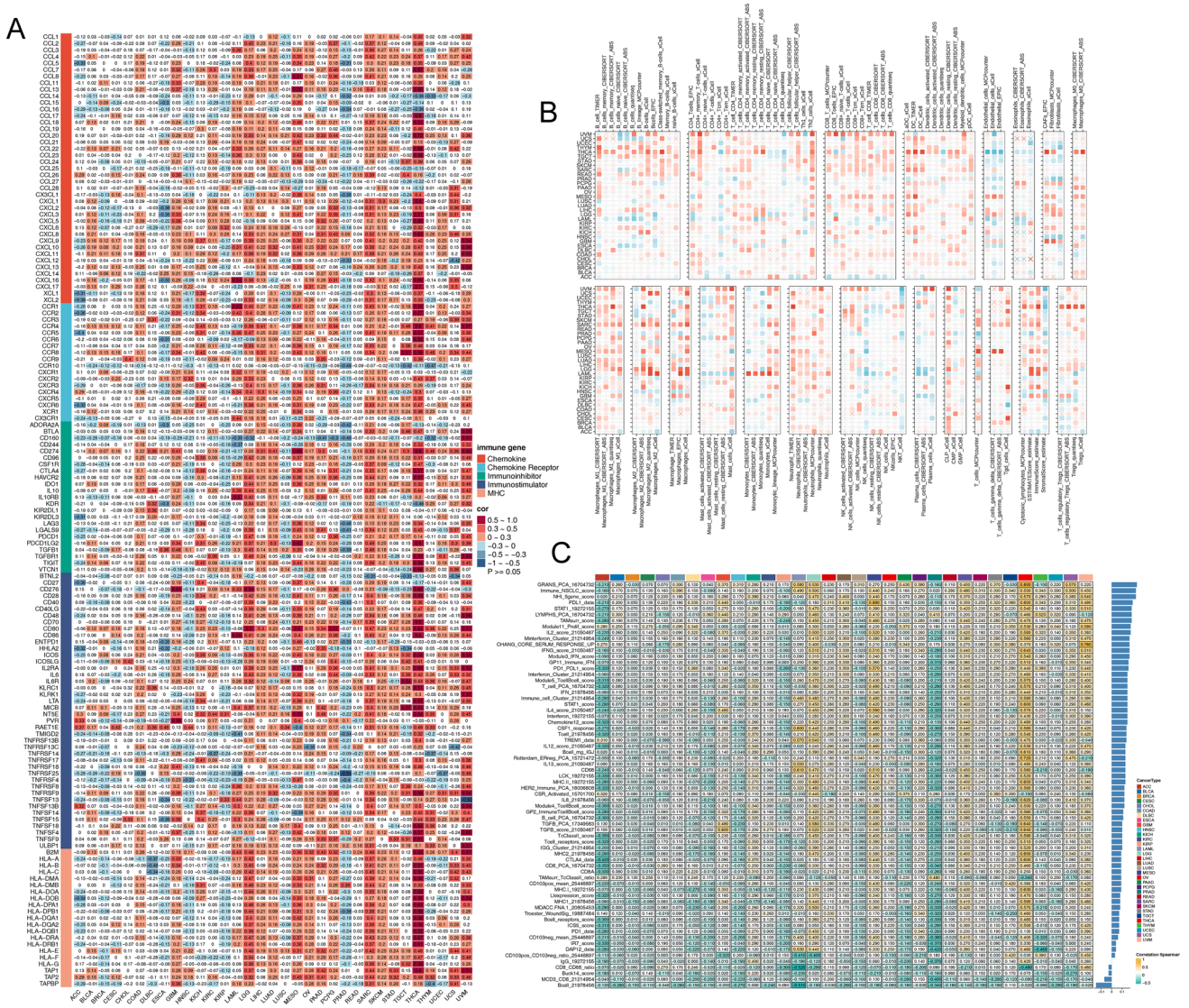

Fig. 4 Correlation of ARF6 with Immune Genes and Cell Infiltration. **A** Pearson correlation of ARF6 with immune genes across cancers. **B** Spearman correlation of ARF6 with immune cell infiltration across cancers. **C** Spearman correlation of ARF6 with 68 immune-related traits. Negative correlations were observed with PD-L1 in PRAD, while positive correlations were found with inflammatory markers.Red indicates positive correlations, blue indicates negative correlations, with deeper colors reflecting stronger correlations

= – 0.68). These findings indicate that ARF6 may suppress immune response pathways in the TME of prostate cancer. However, positive correlations were observed with inflammatory markers such as TNF (r = 0.62), suggesting that ARF6 may also promote pro-inflammatory immune responses in certain contexts. This dual effect underscores the complexity of ARF6's role in regulating immune features within different tumor microenvironments.

3.5 Correlation and mutation landscape of ARF6 in cancer

The correlation between ARF6 expression and several genomic features was assessed using Spearman's correlation and visualized through a radar plot (Fig. 5A). The analysis revealed significant correlations between ARF6 expression and various genomic features, such as Aneuploidy, Homologous Recombination Defects (HRD), Tumor Ploidy, and SNV Neoantigens. ARF6 expression was positively correlated with Aneuploidy (r = 0.72, p < 0.0001), indicating that increased chromosomal instability may drive higher expression of ARF6 in tumor cells. A similar positive correlation was observed with HRD (r = 0.65, p < 0.001), suggesting that ARF6 could be linked to DNA repair defects in various cancers. Additionally, ARF6 expression was positively correlated with Tumor Ploidy (r = 0.68, p < 0.01), reflecting a potential regulatory

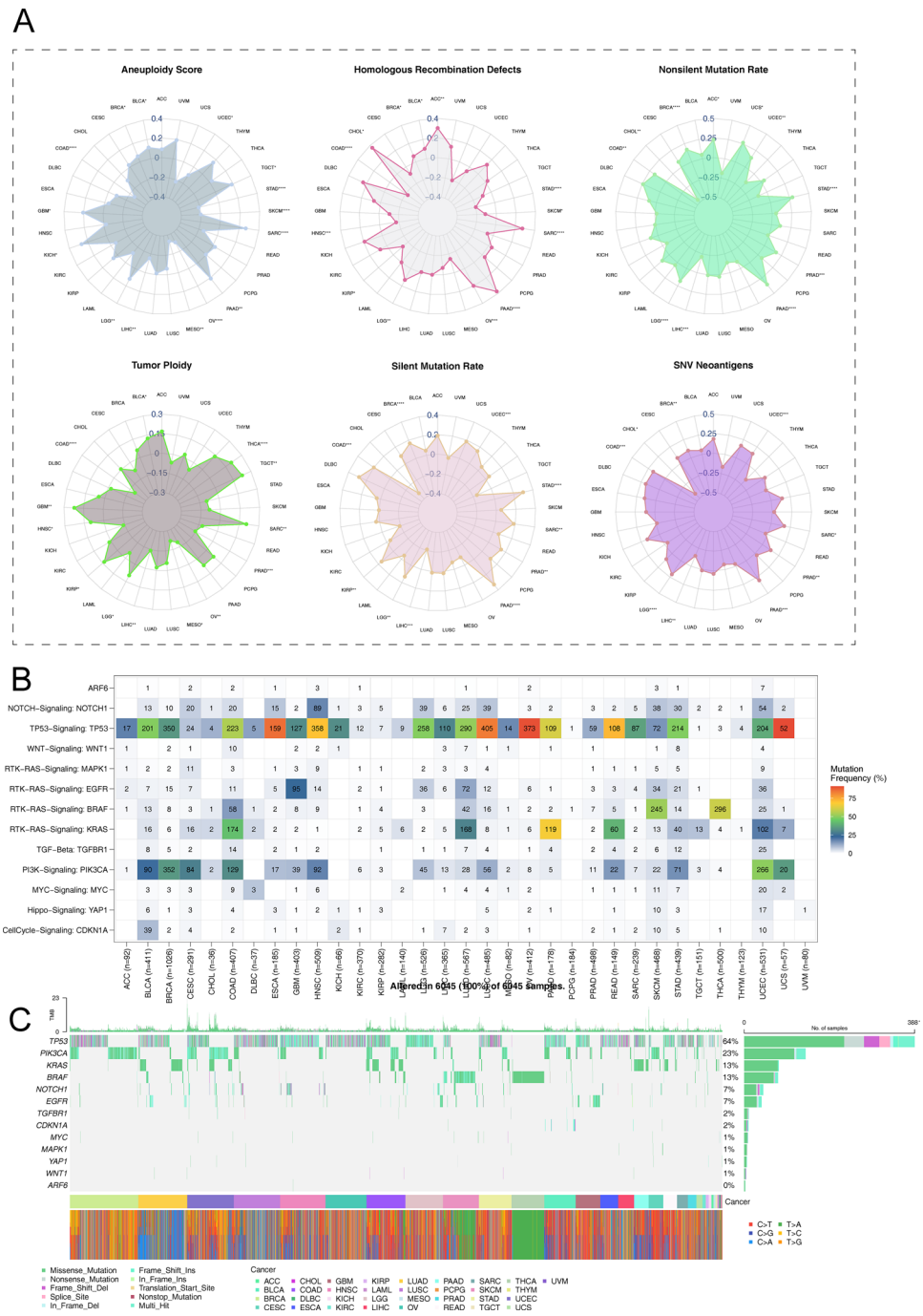

Fig. 5 Correlation and Mutation Landscape of ARF6 in Cancer. **A** Correlation of ARF6 expression with genomic features such as aneuploidy, HRD and tumor ploidy. **B** Mutation frequency of ARF6 in different cancers. **C** Distribution of ARF6 mutations and SNV types in 33 cancer types

relationship between ARF6 expression and chromosomal instability during tumor progression. Conversely, ARF6 expression showed a negative correlation with Silent Mutation Rate ($r = -0.55$, $p < 0.05$), which could imply that higher ARF6 expression might influence the accumulation of non-silent mutations, thus affecting the tumor's mutational landscape. Then, the distribution of ARF6 mutations across different cancers was examined, with a focus on its involvement in classic cancer signaling pathways (Fig. 5B). The bar plot displays the proportion of patients with mutations in ARF6 and associated cancer pathways across various tumor types. The color gradient indicates the proportion of mutant samples, with red representing a higher proportion of mutations. In prostate cancer (PRAD), ARF6 mutations were found in approximately 10% of cases, with a notable enrichment of mutations in key cancer-related signaling pathways, such as the PI3K/AKT and MAPK pathways. This suggests that ARF6 may play a significant role in modulating these pathways in PRAD, potentially influencing tumor progression and response to targeted therapies. Finally, the mutation landscape of ARF6

across 33 cancer types was visualized using an oncoplot (Fig. 5C). The waterfall plot illustrates the distribution of ARF6 mutations and the types of single-nucleotide variations (SNVs) identified in different cancers, with data derived from 8663 TCGA samples. The most common mutation type in ARF6 was missense mutations (46%), followed by silent mutations (32%), which were found across a broad range of cancers. In PRAD, ARF6 mutations were predominantly missense mutations, with several cases exhibiting high variant frequencies in the gene's coding region. These findings underscore the potential oncogenic role of ARF6 mutations in the development and progression of various cancers, particularly in PRAD.

3.6 Correlation of ARF6 expression with chemotherapy sensitivity

The correlation between ARF6 expression and the sensitivity to various chemotherapy drugs was assessed across different cancer types, with the results visualized in a bubble plot (Fig. 6A). The x-axis represents different chemotherapy drugs, while the y-axis corresponds to different chemotherapy drug datasets. Each bubble in the plot represents the Spearman correlation between ARF6 expression and the response to a specific chemotherapy drug. The color of the bubble indicates the direction of the correlation, with red representing positive correlations and blue representing negative correlations, and the color intensity reflecting the strength of the correlation. The analysis revealed that ARF6 expression was strongly positively correlated with the response to platinum-based chemotherapy drugs (e.g., cisplatin), particularly in prostate cancer (PRAD) ($r = 0.78$, $p < 0.001$), suggesting that higher ARF6 expression may enhance the sensitivity to these drugs. Additionally, a negative correlation was observed between ARF6 expression and the response to some chemotherapeutic agents, such as taxanes, in cancers like breast cancer ($r = -0.65$, $p < 0.01$), indicating that high ARF6 expression might reduce the effectiveness of certain chemotherapies. In Fig. 6B, a heatmap visualization was used to assess the relationship between ARF6 expression and chemotherapy response across multiple tumor types. The heatmap clearly illustrates the differential sensitivity of various tumors to chemotherapy drugs based on ARF6 expression levels. Prostate cancer (PRAD) displayed a notable sensitivity to cisplatin, with a high correlation between ARF6 expression and drug efficacy, highlighting ARF6 as a potential predictive biomarker

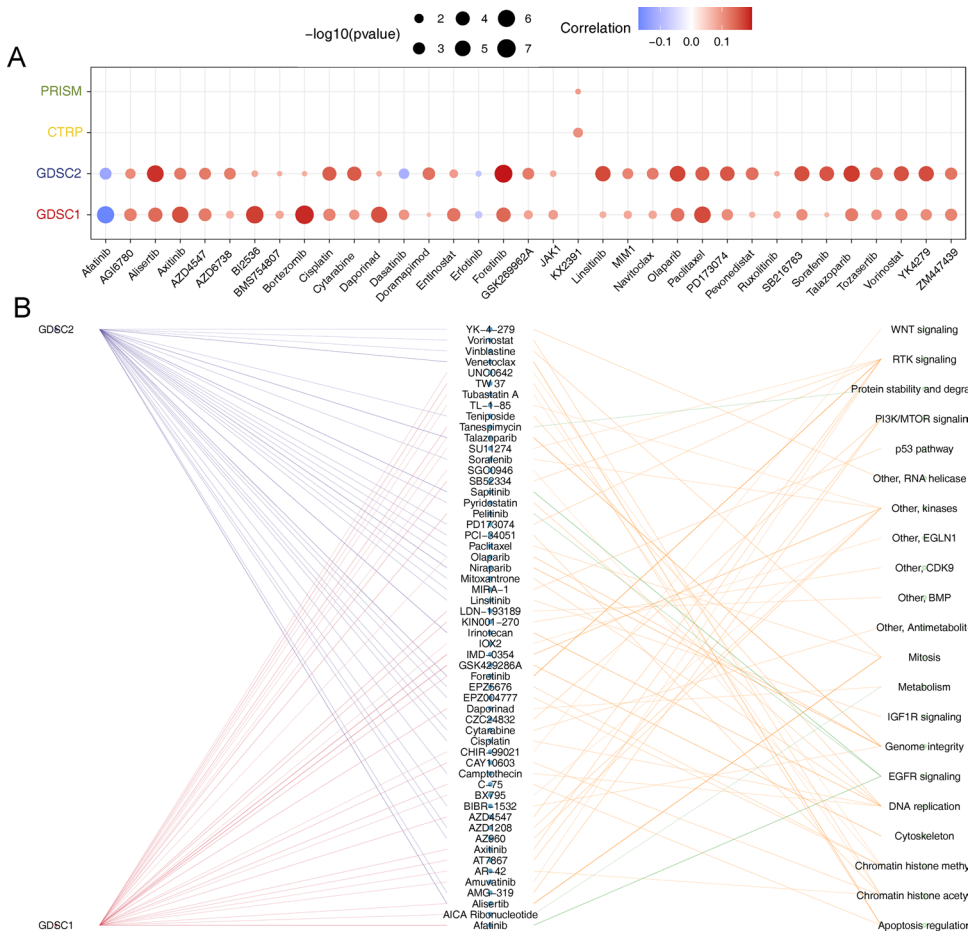

Fig. 6 Correlation of ARF6 Expression with Chemotherapy Sensitivity. **A** The Spearman correlation between ARF6 expression and chemotherapy response across various cancer types. Red and blue indicate positive and negative correlations, respectively, with color intensity representing the strength of the correlation. **B** The relationship between ARF6 expression and chemotherapy sensitivity in different tumors

for platinum-based therapy response. On the other hand, tumors such as lung adenocarcinoma (LUAD) and breast cancer showed a weaker correlation with ARF6 expression and chemotherapeutic efficacy, particularly for taxanes and anthracyclines. These results suggest that ARF6 may influence chemotherapy response in a tumor-specific manner, potentially offering insights into how ARF6 could be leveraged to personalize chemotherapy regimens, especially in tumors like PRAD that show a stronger relationship with platinum-based drugs.

3.7 Chromatin accessibility landscape of ARF6 revealed by ATAC-seq analysis

The analysis of ATAC-seq data for ARF6 revealed distinct patterns of chromatin accessibility across chromosomes, providing insights into the regulatory landscape of this gene. The distribution of ATAC-seq peaks across chromosomes was uneven, indicating varying degrees of chromatin openness in different genomic regions (Fig. 7A). This suggests that certain chromosomal regions are more accessible and potentially more active in terms of transcriptional regulation. The size distribution of these peaks showed a specific pattern, with a range of peak sizes reflecting the diversity in chromatin accessibility (Fig. 7B). Furthermore, the feature distribution analysis highlighted that a significant proportion of ATAC-seq peaks were located within promoter regions, with 57.95% of peaks found within 1 kb of transcription start sites and an additional 6.68% within 1–2 kb (Fig. 7C). This indicates a strong association of accessible chromatin with gene regulatory elements. Additionally, 7.95% of peaks were located in the 3'UTR regions, while 2.27% were found in the first exon, and 26.14% were distributed across other intronic regions. This distribution underscores the importance of both promoter and intragenic regions in the regulation of ARF6 expression. Overall, these findings provide a comprehensive view of the chromatin accessibility landscape associated with ARF6, highlighting key regulatory regions that may play a crucial role in its transcriptional regulation.

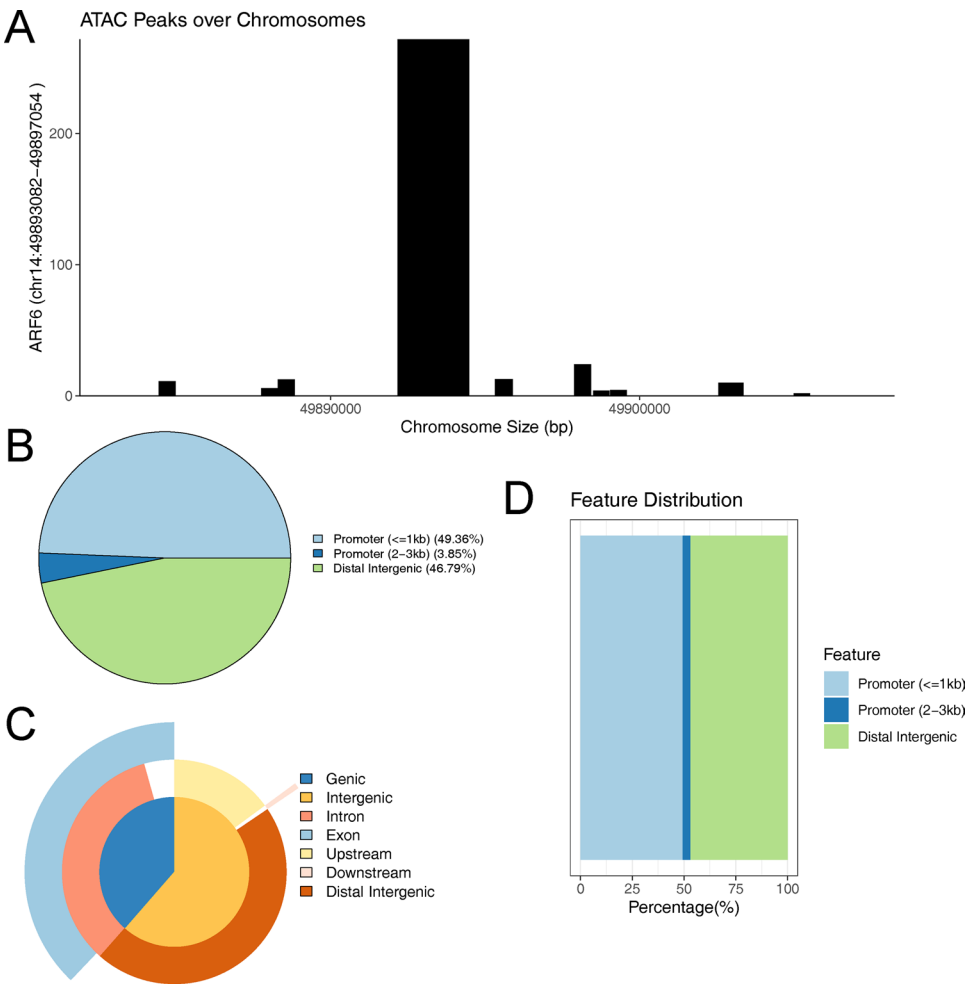

Fig. 7 Distribution and characteristics of ATAC-seq peaks associated with ARF6. **A** Chromosomal distribution of ATAC-seq peaks, showing uneven accessibility across genomic regions. **B** Size distribution of ATAC-seq peaks, reflecting variability in chromatin openness. **C** Feature distribution of ATAC-seq peaks, highlighting enrichment in promoter and intragenic regions. Percentages indicate the proportion of peaks located in specific genomic features. **D** Detailed classification of ATAC-seq peaks across genic, intergenic, intron, exon, upstream, downstream, and distal intergenic regions

3.8 Correlation between ARF6 expression and functional states in cancer cells

We explored the correlation between ARF6 expression and various functional states of cancer cells, as defined by the CancerSEA database. The results are depicted in a scatter plot where the y-axis represents the standardized z-scores for each functional state, and the x-axis shows the z-score of ARF6 gene expression. Different colors on the plot correspond to different functional state types, providing a clear visualization of the relationships between ARF6 expression and these states (Fig. 8). Pearson correlation coefficients (R) were calculated to assess the strength and direction of the relationships. We used a z-score algorithm, based on the method proposed by Lee et al., and applied it to 14 functional state gene sets from the CancerSEA database to obtain combined z-scores. These scores were further standardized using the scale function to define gene set scores, which were then correlated with ARF6 expression via Pearson analysis. The results revealed significant correlations between ARF6 expression and certain functional states, suggesting that ARF6 may be involved in regulating specific tumor cell behaviors. Notably, strong positive or negative correlations were observed with specific functional states, indicating ARF6's potential role in modulating cellular processes such as proliferation, migration, and invasion. These findings offer insights into how ARF6 expression might influence the functional heterogeneity of cancer cells.

3.9 Expression characteristics and clinical significance of ARF6 in PRAD

Given that in the pan-cancer analysis we found that ARF6 has specific significance in PRAD at multiple levels. In the TCGA-PRAD dataset, we first performed a pairwise difference analysis of the expression differences of ARF6 gene between PRAD tumor tissues and normal tissues. The results showed that the expression of ARF6 gene was significantly higher in tumor tissues than in the corresponding paracancerous tissues (Fig. 9A). The difference in expression levels between tumor and paracancerous tissues was statistically significant when compared by the Wilcoxon signed rank test, suggesting that ARF6 may play an important role in the tumorigenesis and development of PRAD. Further analysis was based on tumor versus normal tissues in the TCGA-PRAD dataset using the Wilcoxon rank sum test. The results showed that the expression of ARF6 was significantly higher in tumor tissues than in normal tissues (Fig. 9C). In the statistical plots, the upper and lower interquartile ranges of the boxes showed the expression differences between the two groups, and the expression levels in the tumor group were significantly higher than those in the normal group, further confirming the high expression pattern of ARF6 in PRAD. To evaluate the diagnostic performance of ARF6 gene in PRAD, we performed ROC curve analysis. This analysis showed that ARF6 performed with high accuracy in distinguishing the tumor group from the normal group, with an AUC value of 0.792 and a 95% confidence interval of 0.726–0.851 (Fig. 9D). This result suggests that the ARF6 gene has a strong diagnostic value in PRAD and can effectively differentiate between tumor and

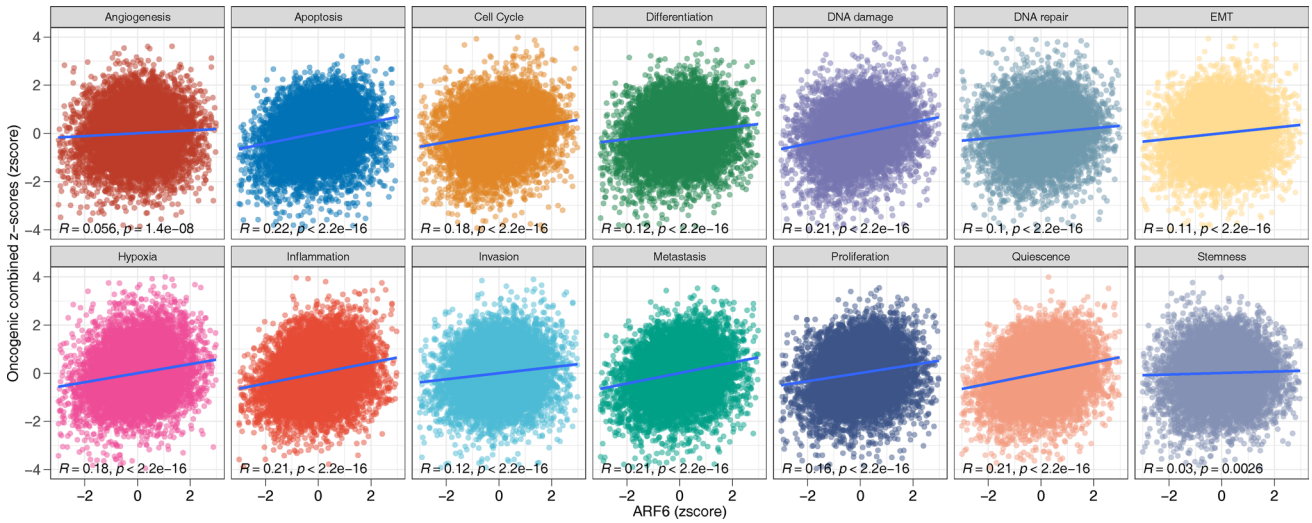

Fig. 8 The correlation between ARF6 expression and various cancer cell functional states is shown, with ARF6 expression on the x-axis and the combined z-scores of functional states on the y-axis. Different colors represent different functional states. Pearson correlation coefficients (R) were calculated for each functional state

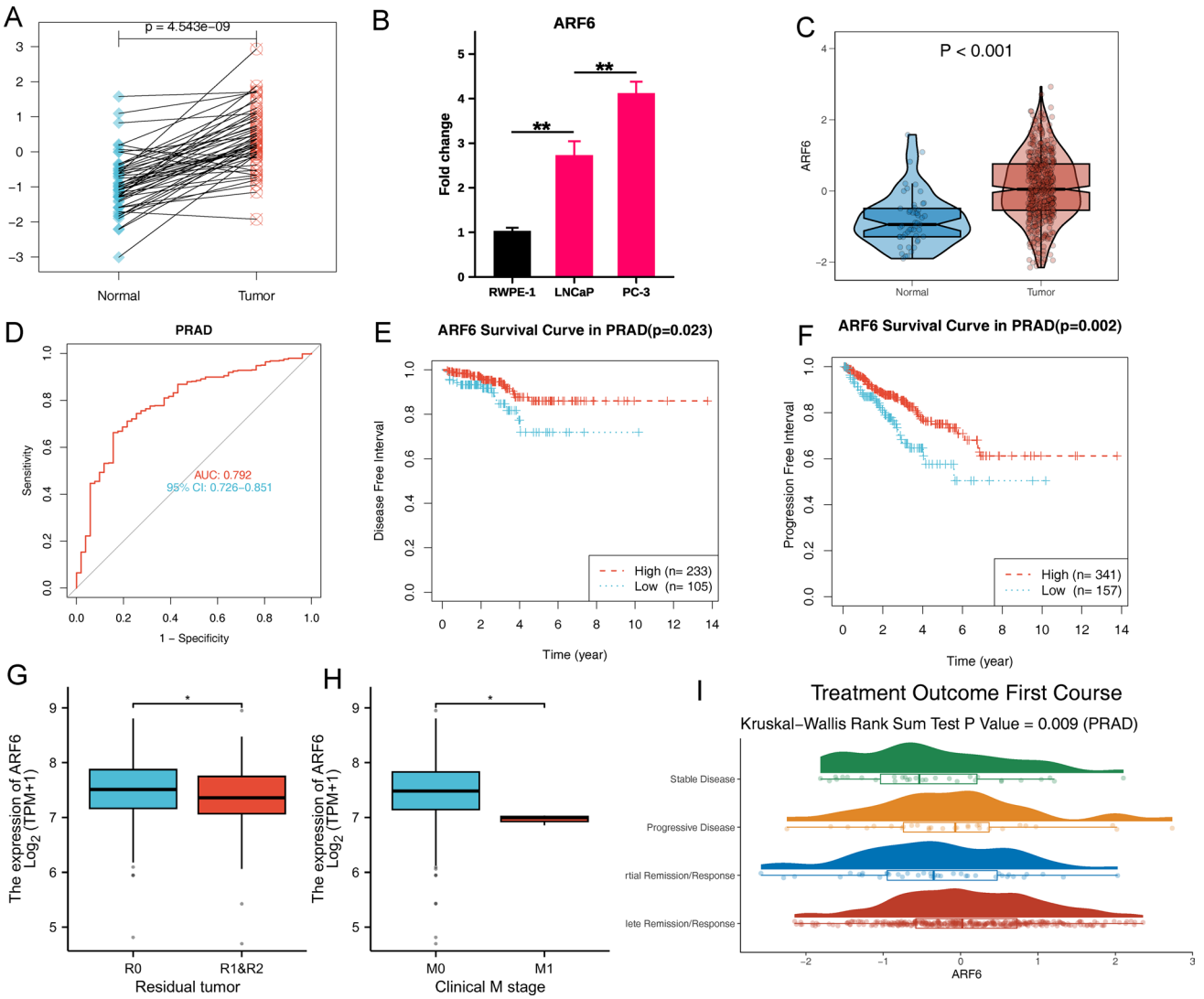

Fig. 9 **A** Differential expression of ARF6 between PRAD tumor tissues and adjacent normal tissues (Wilcoxon signed-rank test). **B** RT-qPCR validation of ARF6 mRNA expression in prostate cancer cell lines (LNCaP and PC- 3) compared to normal prostate epithelial cells (NC, RWPE-1), showing fold changes of 2.7 and 4.1, respectively (Student's t-test, ** $p < 0.01$ for LNCaP vs. NC, *** $p < 0.001$ for PC- 3 vs. NC). **C** Differential expression of ARF6 between PRAD tumor tissues and normal tissues (Wilcoxon rank-sum test). **D** ROC curve analysis of ARF6 for distinguishing tumor from normal tissues (AUC = 0.792). **E** and **F** Kaplan–Meier survival analysis comparing disease-free interval (DFI) and progression-free interval (PFI) between ARF6 high-expression and low-expression groups. **G** Differential expression of ARF6 in residual tumor groups. **H** Differential expression of ARF6 in metastatic stages (M1 vs. M0) of PRAD. **I** Differential expression of ARF6 in groups with different treatment responses

normal tissues. Next, we evaluated the relationship between the expression level of ARF6 gene and the prognosis of PRAD patients using Kaplan–Meier survival curve analysis. The results showed that there was a significant difference in the survival curves between the ARF6 high-expression group and the low-expression group, with the high-expression group having inferior DFI and PFI than the low-expression group (Fig. 9D and 9E, $p < 0.05$). This suggests that high expression of ARF6 is associated with poorer prognosis and may serve as a potential biomarker for the prognosis of PRAD patients. Not only that, there were significant differences in the expression of ARF6 gene in different residual tumor groups. Specifically, ARF6 expression was significantly higher in the group of patients with residual tumors than in the group of patients without residual tumors. This difference was shown to be significant by statistical test ($p < 0.05$), implying that ARF6 may be associated with residual and recurrent tumors, and that high expression of ARF6 may suggest incomplete resection of the tumor or risk of recurrence. In the staging analysis, there was a significant difference in the expression of ARF6 in the M1 stage versus the M0 stage (Fig. 9H), suggesting that ARF6 may be directly involved in the process of metastatic stage of PRAD. In further analysis of patients with different treatment responses, we found that ARF6 expression was

higher in the progressive disease group versus the stable disease group, and lower in the partial remission group versus the complete remission group (Fig. 9I). These results suggest that high ARF6 expression may be associated with poor treatment response, suggesting that it may have an important predictive role in the clinical management of the disease.

3.10 Correlation analysis of ARF6 with the immune microenvironment of prostate cancer

We further evaluated the relationship between high ARF6 expression and immune-related features of prostate cancer (PRAD). First, Fig. 10A showed that the MeTIL level in the ARF6 high expression group was significantly higher than that in the low expression group ($P < 0.001$), suggesting that high expression of ARF6 may be associated with changes in tumor methylation characteristics. Further analyzing the expression of genes related to immune response, Fig. 10B showed that the ARF6 high-expression group was not significantly different from the low-expression group in the expression of IFN-γ ($P = 0.418$), suggesting a weaker association between ARF6 and IFN-γ. In contrast, Fig. 10C demonstrated that the T-cell inflammatory response was significantly stronger in the high-expression group than in the low-expression group ($P < 0.001$), suggesting that ARF6 may enhance the immune response by promoting T-cell-mediated inflammatory response.

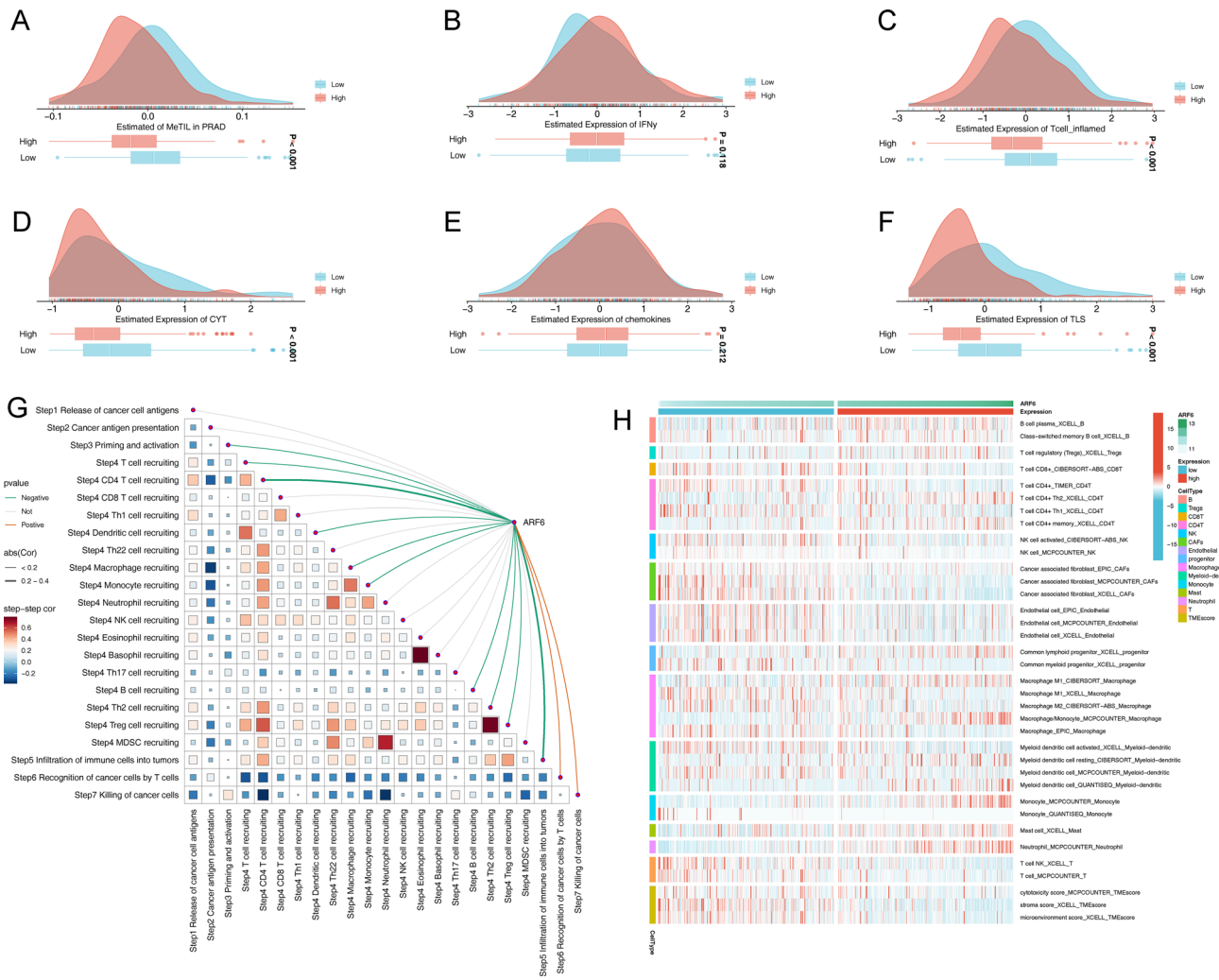

Fig. 10 Relationship between ARF6 and immune-related features of prostate cancer (PRAD). **A** MeTIL levels were significantly higher in the ARF6 high-expression group ($P < 0.001$); **B** there was no significant difference in IFN-γ expression ($P = 0.418$); **C** T-cell inflammatory response was significantly enhanced ($P < 0.001$); (D) CYT levels were significantly higher ($P < 0.001$); **E** the difference in chemokine expression was not significant ($P = 0.212$); **F** Significantly increased expression of tumor-associated lymphoid structures (TLS) ($P < 0.001$); **G** Correlation of ARF6 with immune cell recruitment and immune response steps; **H** Multi-dimensional heatmap analysis of ARF6 expression with different immune cell infiltration

In addition, Fig. 10D showed that the CYT level in the ARF6 high-expression group was significantly higher than that in the low-expression group ($P < 0.001$), further supporting the potential role of ARF6 in enhancing tumor immune response. In contrast, Fig. 10E showed that the difference in chemokine expression between the ARF6 high-expression group and the low-expression group was small and did not reach significance ($P = 0.212$), suggesting that ARF6 had a weak regulatory effect on chemokine expression. Figure 10F further showed that the high-expression group was significantly higher than the low-expression group in the expression of tumor-associated lymphoid structures (TLS) ($P < 0.001$), suggesting that ARF6 may enhance the immune response by promoting the formation of lymphoid structures in the tumor microenvironment, and then enhance the immune response.

In terms of the tumor immune microenvironment, we explored the relationship between ARF6 and immune cell recruitment and immune response. Figure 10G showed that ARF6 was significantly correlated with several immune response steps (e.g., cancer cell antigen release, antigen presentation, T cell activation, and immune cell recruitment), and in particular, ARF6 expression was positively correlated with the recruitment of T cells, B cells, and natural killer (NK) cells, suggesting that ARF6 may play a key role in promoting tumor infiltration by immune cells. In addition, a strong correlation was also shown between ARF6 and immune responses of T cells and macrophages, suggesting that its high expression may enhance tumor immune responses and influence the infiltration pattern of immune cells in the tumor microenvironment.

Figure 10H further demonstrates the specific relationship between ARF6 expression and different immune cell types through a multidimensional heat map. We found that there were significant differences in the distribution and infiltration characteristics of immune cells in the ARF6 high expression group. Specifically, high ARF6 expression was closely associated with the infiltration of B cells, CD8 + T cells, CD4 + T cells, and NK cells, and was also significantly associated with the expression of immune cells such as macrophages and dendritic cells. These results suggest that ARF6 plays an important role in the tumor immune microenvironment and may influence the immune response and prognosis of tumors by regulating the recruitment and activation of immune cells.

3.11 Functional enrichment analysis of ARF6 in prostate cancer

To elucidate the potential roles and pathways of ARF6 in prostate cancer, we performed Gene Set Enrichment Analysis (GSEA) for both Gene Ontology (GO) and Kyoto Encyclopedia of Genes and Genomes (KEGG) pathways. The GSEA-GO analysis revealed significant enrichment of biological processes related to protein localization and translation regulation, including"Positive regulation of establishment of protein localization to chromosome"(p.adjust = 0.001) and"Regulation of translational initiation in response to stress"(p.adjust = 0.002) (Fig. 11A). These findings suggest that ARF6 may play a critical role in modulating protein trafficking and stress-responsive translational mechanisms in prostate cancer cells.

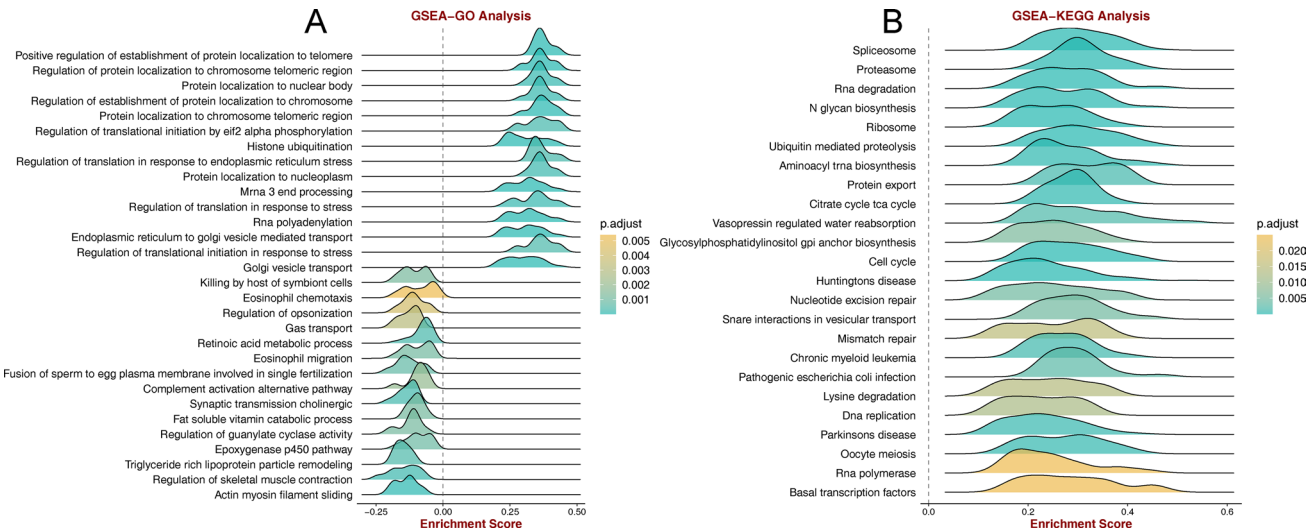

Fig. 11 GSEA-GO and GSEA-KEGG analysis of ARF6 in prostate cancer. **A** Enriched GO terms related to protein localization, translation regulation, and epigenetic processes. **B** Enriched KEGG pathways, including spliceosome, proteasome, and cell cycle regulation. Adjusted p-values are indicated for significant terms and pathways

Additionally, processes such as"Histone biotinylation"(p.adjust = 0.004) and"Ras polysialylation"(p.adjust = 0.005) were also enriched, indicating potential involvement in epigenetic regulation and Ras signaling pathways.

The GSEA-KEGG analysis further identified key pathways associated with ARF6, including"Spliceosome"(p.adjust = 0.005),"Proteasome"(p.adjust = 0.010), and"Ubiquitin-mediated proteolysis"(p.adjust = 0.015), highlighting its potential role in RNA processing, protein degradation, and cellular homeostasis (Fig. 11B). Notably, pathways such as"Cell cycle"(p.adjust = 0.020) and"DNA replication"(p.adjust = 0.015) were also enriched, suggesting that ARF6 may influence cell proliferation and genomic stability in prostate cancer. These results collectively underscore the multifaceted role of ARF6 in regulating critical cellular processes and pathways implicated in prostate cancer progression.

3.12 Experimental validation of ARF6 expression in PCa cell lines

To confirm the bioinformatics prediction of ARF6 overexpression in PCa, we performed RT-qPCR analysis on prostate cancer cell lines (LNCaP and PC- 3) and a normal prostate cell line (RWPE- 1). The results revealed significantly higher ARF6 mRNA expression in both LNCaP (2.7-fold, $p < 0.001$) and PC- 3 (4.1-fold, $p < 0.001$) compared to RWPE- 1 (Fig. 9B). These findings align with the TCGA-based differential expression analysis, where ARF6 was overexpressed in PCa tissues relative to normal tissues. Notably, the more aggressive PC- 3 cell line, derived from metastatic PCa, exhibited a higher fold-change in ARF6 expression than LNCaP, which originates from a lymph node metastasis, suggesting a potential correlation between ARF6 levels and PCa aggressiveness. These experimental data provide robust validation of the bioinformatics results, reinforcing ARF6's role as a potential biomarker in PCa.

4 Discussion

Our study demonstrates that ARF6 plays a pivotal role in PCa progression, with significant overexpression in tumor tissues compared to normal controls, particularly in advanced and metastatic stages. This differential expression, validated through multi-omics analysis across various cancer types, was further confirmed by RT-qPCR experiments, which showed 2.7-fold ($p < 0.001$) and 4.1-fold ($p < 0.001$) increases in ARF6 mRNA levels in PCa cell lines LNCaP and PC- 3, respectively, compared to normal prostate epithelial cells RWPE- 1. These findings, consistent with TCGA data, underscore ARF6's involvement in key biological processes, including Methuosis-mediated cell death, immune regulation, and chemotherapy sensitivity. Notably, the strong negative correlation between ARF6 and immune checkpoint markers like PD-L1 ($r = -0.74$), alongside its prognostic significance ($p < 0.05$), highlights its potential as a multifaceted biomarker in PCa, influencing both tumor behavior and therapeutic response.

Our analysis demonstrated that ARF6 expression is significantly elevated in prostate cancer tissues compared to normal tissues, suggesting its potential as a diagnostic marker. The ROC curve analysis further supported this, showing high diagnostic accuracy for ARF6 in distinguishing prostate cancer from normal tissues. Additionally, ARF6 expression was strongly associated with tumor progression and poor prognosis, as evidenced by Kaplan–Meier survival analysis, where high ARF6 expression correlated with inferior disease-free interval (DFI) and progression-free interval (PFI). These findings align with previous studies that have implicated ARF6 in tumorigenesis and metastasis, particularly through its role in cellular trafficking and membrane dynamics [26–28]. The elevated expression of ARF6 in metastatic stages (M1) and its association with residual tumors further underscore its potential as a prognostic biomarker in prostate cancer.

The tumor microenvironment (TME) plays a crucial role in cancer progression and therapy resistance [29–31]. Our single-cell and spatial transcriptomic analyses revealed that ARF6 expression is highly heterogeneous within the TME, particularly in prostate cancer. ARF6 was notably upregulated in tumor cell subpopulations, suggesting its involvement in tumor cell migration and immune evasion mechanisms. Furthermore, ARF6 expression correlated with immune cell infiltration, particularly CD8 + T cells, macrophages, and dendritic cells, indicating its potential role in modulating anti-tumor immunity [32]. However, ARF6 also exhibited negative correlations with immunosuppressive markers such as PD-L1 and TGFB1, suggesting a complex dual role in immune regulation. These findings highlight the potential of ARF6 as a target for immunotherapy, particularly in prostate cancer, where immune evasion is a significant barrier to effective treatment [33].

Our analysis of ARF6 expression in relation to chemotherapy sensitivity revealed intriguing insights. ARF6 expression was strongly positively correlated with the response to platinum-based chemotherapy drugs, such as cisplatin, in prostate cancer. This suggests that ARF6 could serve as a predictive biomarker for platinum-based therapy response, potentially guiding personalized treatment strategies. Conversely, ARF6 expression showed a negative correlation with the efficacy of taxanes in breast

cancer, indicating that ARF6 may influence chemotherapy response in a tumor-specific manner. These findings underscore the importance of considering ARF6 expression levels when designing chemotherapy regimens, particularly in prostate cancer.

The ATAC-seq analysis provided valuable insights into the chromatin accessibility landscape of ARF6. The majority of accessible chromatin regions were located within promoter regions, suggesting that ARF6 expression is tightly regulated at the transcriptional level. This regulatory complexity may contribute to the observed heterogeneity in ARF6 expression across different cancer types and stages [34]. The enrichment of accessible regions in promoter and intragenic regions further highlights the potential for ARF6 to be regulated by a variety of transcriptional and epigenetic mechanisms, which could be targeted in future therapeutic strategies [35].

Our exploration of ARF6 expression in relation to functional states of cancer cells revealed significant correlations with processes such as proliferation, migration, and invasion. These findings suggest that ARF6 may play a critical role in modulating the functional heterogeneity of cancer cells, particularly in prostate cancer. The strong positive correlations with cell cycle and DNA replication pathways further support the notion that ARF6 is involved in key cellular processes that drive tumor progression.

While our study provides comprehensive insights into the role of ARF6 in prostate cancer, several limitations should be acknowledged. First, the majority of our analyses were based on publicly available datasets, which may have inherent biases and limitations. Future studies should validate these findings using independent cohorts and experimental models. Second, the mechanistic understanding of ARF6 in Methuosis and its interaction with other cellular pathways remains incomplete. Further functional studies are needed to elucidate the precise mechanisms by which ARF6 regulates Methuosis and its impact on tumor biology. Finally, the potential of ARF6 as a therapeutic target warrants further investigation, particularly in the context of immunotherapy and chemotherapy resistance.

5 Conclusion

In conclusion, our study highlights the multifaceted role of ARF6 in prostate cancer, demonstrating its potential as a diagnostic, prognostic, and therapeutic marker. The differential expression of ARF6 across cancer types, its involvement in immune regulation, and its influence on chemotherapy sensitivity underscore its importance in cancer biology. These findings pave the way for future research aimed at leveraging ARF6 as a target for personalized cancer therapy, particularly in prostate cancer, where effective treatment options for advanced stages are urgently needed.

Author contributions ZD, YY and LQ conceived and designed the study. YY, CY and QL analyzed data. CY, QL and WX collected data. YY and WX analyzed and visualized the data. ZD and YY helped with the final revision of this manuscript. All authors reviewed and approved the final manuscript.

Funding This work was supported by the Fundamental Research Funds for the Central Universities (Lzujbky- 2023-ct06).

Data availability No datasets were generated or analysed during the current study.

Declarations

Competing interests The authors declare no competing interests.

Open Access This article is licensed under a Creative Commons Attribution-NonCommercial-NoDerivatives 4.0 International License, which permits any non-commercial use, sharing, distribution and reproduction in any medium or format, as long as you give appropriate credit to the original author(s) and the source, provide a link to the Creative Commons licence, and indicate if you modified the licensed material. You do not have permission under this licence to share adapted material derived from this article or parts of it. The images or other third party material in this article are included in the article's Creative Commons licence, unless indicated otherwise in a credit line to the material. If material is not included in the article's Creative Commons licence and your intended use is not permitted by statutory regulation or exceeds the permitted use, you will need to obtain permission directly from the copyright holder. To view a copy of this licence, visit http://creativecommons.org/licenses/by-nc-nd/4.0/.

References

1. Wang G, Zhao D, Spring DJ, DePinho RA. Genetics and biology of prostate cancer. Genes Dev. 2018;32(17–18):1105–40.
2. Nguyen-Nielsen M, Borre M. Diagnostic and therapeutic strategies for prostate cancer. Semin Nucl Med. 2016;46(6):484–90.

3. Sekhoacha M, Riet K, Motloung P, Gumenku L, Adegoke A, Mashele S. Prostate cancer review: genetics, diagnosis, treatment options, and alternative approaches. Molecules (Basel, Switzerland). 2022. https://doi.org/10.3390/molecules27175730.
4. Kumar Am S, Rajan P, Alkhamees M, Holley M, Lakshmanan VK. Prostate cancer theragnostics biomarkers: an update. Investigative and clinical urology. 2024;65(6):527–39.
5. Almeeri MNE, Awies M, Constantinou C. Prostate cancer, pathophysiology and recent developments in management: a narrative review. Curr Oncol Rep. 2024;26(11):1511–9.
6. Zhu M, Liu D, Liu G, Zhang M, Pan F. Caspase-linked programmed cell death in prostate cancer: from apoptosis, necroptosis, and pyroptosis to PANoptosis. Biomolecules. 2023. https://doi.org/10.3390/biom13121715.
7. Cheng B, Tang C, Xie J, Zhou Q, Luo T, Wang Q, Huang H. Cuproptosis illustrates tumor micro-environment features and predicts prostate cancer therapeutic sensitivity and prognosis. Life Sci. 2023;325: 121659.
8. Denmeade SR, Lin XS, Isaacs JT. Role of programmed (apoptotic) cell death during the progression and therapy for prostate cancer. Prostate. 1996;28(4):251–65.
9. Elmore S. Apoptosis: a review of programmed cell death. Toxicol Pathol. 2007;35(4):495–516.
10. Pistritto G, Trisciuoglio D, Ceci C, Garufi A, D'Orazi G. Apoptosis as anticancer mechanism: function and dysfunction of its modulators and targeted therapeutic strategies. Aging. 2016;8(4):603–19.
11. Liu S, Yao S, Yang H, Liu S, Wang Y. Autophagy: regulator of cell death. Cell Death Dis. 2023;14(10):648.
12. Eckert AW, Maurer P, Meyer L, Kriwalsky MS, Rohrberg R, Schneider D, Bilkenroth U, Schubert J. Bisphosphonate-related jaw necrosis–severe complication in maxillofacial surgery. Cancer Treat Rev. 2007;33(1):58–63.
13. Maltese WA, Overmeyer JH. Methuosis: nonapoptotic cell death associated with vacuolization of macropinosome and endosome compartments. Am J Pathol. 2014;184(6):1630–42.
14. Luo Y, Guan B, Deng X, Bai P, Huang H, Miao C, Sun A, Li Z, Yang D, Wang X, et al. Methuosis inducer SGI-1027 cooperates with everolimus to promote apoptosis and pyroptosis by triggering lysosomal membrane permeability in renal cancer. Adv Sci (Weinheim Baden-Wurttemberg, Germany). 2024;11(38):2404693.
15. Bielsa N, Casasampere M, Abad JL, Enrich C, Delgado A, Fabriàs G, Lizcano JM, Casas J. Methuosis contributes to Jaspine-B-induced cell death. Int J Mol Sci. 2022. https://doi.org/10.3390/ijms23137257.
16. Ritter M, Bresgen N, Kerschbaum HH. From pinocytosis to Methuosis-fluid consumption as a risk factor for cell death. Front Cell Dev Biol. 2021;9: 651982.
17. Chen Y, Liu S, Wei Y, Wei H, Yuan X, Xiong B, Tang M, Yang T, Yang Z, Ye H, et al. Discovery of potent and selective phosphatidylinositol 3-phosphate 5-kinase (PIKfyve) inhibitors as Methuosis inducers. J Med Chem. 2024;67(1):165–79.
18. Qiu Z, Liu W, Zhu Q, Ke K, Zhu Q, Jin W, Yu S, Yang Z, Li L, Sun X, et al. The role and therapeutic potential of macropinocytosis in cancer. Front Pharmacol. 2022;13: 919819.
19. Ye T, Shan P, Zhang H. Progress in the discovery and development of small molecule Methuosis inducers. RSC Med Chem. 2023;14(8):1400–9.
20. Kim D, Min D, Kim J, Kim MJ, Seo Y, Jung BH, Kwon SH, Ro H, Lee S, Sa JK, et al. Nutlin-3a induces KRAS mutant/p53 wild type lung cancer specific methuosis-like cell death that is dependent on GFPT2. Journal of Exp Clin Cancer Res CR. 2023;42(1):338.
21. Bhanot H, Young AM, Overmeyer JH, Maltese WA. Induction of nonapoptotic cell death by activated Ras requires inverse regulation of Rac1 and Arf6. Mol Cancer Res MCR. 2010;8(10):1358–74.
22. Gamara J, Davis L, Leong AZ, Pagé N, Rollet-Labelle E, Zhao C, Hongu T, Funakoshi Y, Kanaho Y, Aoudji F, et al. Arf6 regulates energy metabolism in neutrophils. Free Radical Biol Med. 2021;172:550–61.
23. Sun D, Guo Y, Tang P, Li H, Chen L. Arf6 as a therapeutic target: Structure, mechanism, and inhibitors. Acta Pharmaceutica Sinica B. 2023;13(10):4089–104.
24. Sabe H. KRAS, MYC, and ARF6: inseparable relationships cooperatively promote cancer malignancy and immune evasion. Cell Commun Signal. 2023;21(1):106.
25. Abdul-Salam VB, Russomanno G, Chien-Nien C, Mahomed AS, Yates LA, Wilkins MR, Zhao L, Gierula M, Dubois O, Schaeper U, et al. CLIC4/Arf6 Pathway. Circ Res. 2019;124(1):52–65.
26. Zhang J, Yao Y, Li H, Ye S. miR-28-3p inhibits prostate cancer cell proliferation, migration and invasion, and promotes apoptosis by targeting ARF6. Exp Ther Med. 2021;22(5):1205.
27. Koumakpayi IH, Le Page C, Delvoye N, Saad F, Mes-Masson AM. Macropinocytosis inhibitors and Arf6 regulate ErbB3 nuclear localization in prostate cancer cells. Mol Carcinog. 2011;50(11):901–12.
28. Lei H, Ma F, Jia R, Tan B. Effects of Arf6 downregulation on biological characteristics of human prostate cancer cells. Int Braz J Urol : Offic J Braz Soc Urol. 2020;46(6):950–61.
29. Xiao Y, Yu D. Tumor microenvironment as a therapeutic target in cancer. Pharmacol Ther. 2021;221: 107753.
30. Arneth B: Tumor Microenvironment. *Medicina (Kaunas, Lithuania)* 2019, 56(1).
31. Jin MZ, Jin WL. The updated landscape of tumor microenvironment and drug repurposing. Signal Transduct Target Ther. 2020;5(1):166.
32. Lee S, Ishitsuka A, Kuroki T, Lin YH, Shibuya A, Hongu T, Funakoshi Y, Kanaho Y, Nagata K, Kawaguchi A. Arf6 exacerbates allergic asthma through cell-to-cell transmission of ASC inflammasomes. JCI Insight. 2021. https://doi.org/10.1172/jci.insight.139190.
33. Hashimoto S, Furukawa S, Hashimoto A, Tsutaho A, Fukao A, Sakamura Y, Parajuli G, Onodera Y, Otsuka Y, Handa H, et al. ARF6 and AMAP1 are major targets of KRAS and TP53 mutations to promote invasion, PD-L1 dynamics, and immune evasion of pancreatic cancer. Proc Natl Acad Sci USA. 2019;116(35):17450–9.
34. Li R, Peng C, Zhang X, Wu Y, Pan S, Xiao Y. Roles of Arf6 in cancer cell invasion, metastasis and proliferation. Life Sci. 2017;182:80–4.
35. Garcia-Martinez L, Zhang Y, Nakata Y, Chan HL, Morey L. Epigenetic mechanisms in breast cancer therapy and resistance. Nat Commun. 2021;12(1):1786.

Publisher's Note Springer Nature remains neutral with regard to jurisdictional claims in published maps and institutional affiliations.